The Effect of Roof Clearance on Wind Loads for Solar Arrays on a Low-rise Building

Chin-Cheng Chou[1]　　Cheng-Yang Chung[1]　　Kung-Ming Chung[2*]

ABSTRACT

The building code in Taiwan requires that the maximum height of a Photovoltaic (PV) system must be less than 6 m above the top of a flat roof. However, Taiwan is situated in the prevalent typhoon track in the northwestern Pacific. Wind loading on PV systems is an essential concern for design. This paper reports an experimental study of tilted solar arrays (tilt angle = 25°, 6 rows) on a low-rise building. The tests are conducted in a boundary layer wind tunnel at a scale of 1:20. Mean and fluctuating pressure coefficients are computed for every pressure tap. The normal force coefficient is also evaluated for each array. When facing into the direction of the wind, the normal force is greatest on the first array and there is sheltering effect on the second to sixth arrays. However, peak pressure fluctuations on the second array are observed. Wind-induced vibrations require caution. An increase in roof clearance results in a greater normal force on the first array, in which there is a 30% increase. Pressure fluctuations of greater amplitude are also observed on the second to sixth arrays. The fluctuating pressure coefficient reaches a peak value of 0.62 on the lower surface of the second array.

Keywords: roof clearance, wind load, solar arrays, low-rise building, renewable energy.

1. Introduction

The use of fossil fuels results in a green house effect and environmental pollution. The Paris Agreement aims to limit carbon emissions and to maintain a global temperature rise of less than 2°C above pre-industrial levels by the end of this century (Voigt, 2016). Renewable energy sources are sustainable, so their use to produce power has received increasing public support. For solar PV, the total capacity in operation was 502 GW in 2018, corresponding to energy supplies of 640 TWh (24.5% of global renewable energy supply) (Mauthner and Spörk-Dür, 2019). In Taiwan, 98% of the energy that is produced relies on the importation of fuel (BOEMOEA, 2017). To ensure balanced development in energy security and environmental sustainability, the Renewable Energy Development Bill was enacted in 2010. The proportion of the total energy requirement that is generated using renewable energy is expected to be 20% by 2025. It is also expected that solar PV installed capacity will be 20 GW (BOEMOEA, 2016). Feed-in tariffs for renewable energy electric power (20-year electric power procurement) have been initiated.

A ground-mounted solar (PV or thermal) system consists of tilted panels and is prone to extreme wind loads. In a uniform flow, Chung *et al*. (2011) showed that there are strong suction

forces near the front edge on the upper surface and slight variation in the mean surface pressure on the lower surface. The unit sectional uplift coefficient decreases when tilt angle increases. The mean spanwise pressure distributions have an inverted U-shape, indicating a three-dimensional effect or corner vortices. When the turbulence intensity of the freestream increases, there is an upstream movement of a separation bubble and side-edge vortices (Chung et al., 2013). The effect of wind incidence was studied by Chou et al. (2014). Greater suction on the upper surface near the windward corner is observed, when the wind direction is 15°–60°. The tilted panels shed vortices (Matty, 1979; Chen & Fang, 1996), which create a peak in the turbulence and excitation spectra on the second row panels (Strouhal number ≈ 0.15). There is a decrease in buffeting as the distance into array increases (Strobel & Banks, 2014). For roof-mounted solar arrays, Radu and Axinte (1986, 1989) found that the wind loads on tilted panels are significantly reduced by the sheltering effect of the first row panels and of the building itself. The largest wind loads corresponds to vortex shedding from in-line panels and the peak system torque occurs angles of approach for wind that are near the diagonals of the panel (Kopp et al., 2002). Pratt and Kopp (2013) showed that a local flow is established by large-scale vortices that are generated respectively by the building and by the reattachment of a separated shear layer for small tilt angle ($= 2^{o}$) and larger tilt angle ($= 20^{o}$). Kopp et al. (2012) noted that the net loading is due primarily to pressure equalization when the tilt angle is small and to turbulence that is generated by the panels when the tilt angle is large. The study by Cao et al. (2013) demonstrated similar results. In terms of the effect of spacing parameters, Warsido et al. (2014) noted that the wind load

coefficient decreases when perimeter gap from the building edge increases and there is a sheltering effect on the second row panels, which results in a reduction in the force and the moment coefficients.

Designers of a PV system often use wind loading standards, such as American Society Civil Engineers (ASCE) 7 (2010), to calculate wind loads. However, the design must ensure that the system functions properly during extreme wind events, such as typhoons or hurricanes. Stathopoulos et al. (2014) determined the effect of panel inclination (tilt angle), building height and wind direction. The effect of building height appears to be minimal and the effect of panel inclination is significant only for critical wind directions. The effect of roof clearance (the distance between the roof and the panel, h) was studied by Kopp ($h = 0.15$–1.02 m) (2014) and by Naeiji et al. (h $= 0.3$–0.45 m) (2017).

In Taiwan, the "Million Rooftop PVs Project" was initiated by the Bureau of Energy, Ministry of Economic Affair in 2011. PV systems are usually mounted on rooftops of 3-5 story buildings. The building code in Taiwan requires that the maximum height of a PV system must be less than 6 m above the top of a flat roof (Kaohsiung City, 2017). The present study then focuses on the effect of roof clearance and sheltering for a PV system on a low-rise building. Pressure taps installed on tilted panels are used to calculate forces for solar arrays, using a boundary layer wind tunnel.

2. Experimental Setup

Experiments were conducted in a boundary-layer wind tunnel at the Architecture and Building Research Institute (Tainan, Taiwan). The closed-loop tunnel has a honeycomb and three screens. The contraction ratio is 4.71. The constant-area

test section is 2.6 m (height) × 4 m (width) × 36.5 m (length). A schematic drawing of the test configuration is shown in Fig. 1 and the detailed geometry of the test model is shown in Table 1. The tilted solar arrays (6 rows × 10 solar panels, denoted as R1–R6) were installed facing into the direction of the wind on the flat roof of a low-rise building ($B \times D \times H = 10 \times 10 \times 9$ m). Note that the tilt angle of the solar arrays is 25°, corresponding to the local latitude in Taiwan. The height, K, of the solar arrays is 0.69 m. To determine the effect of roof clearance on wind loads for solar arrays, the total height of the solar arrays ($= h + K$) was set at 1, 2 and 3 m, which values correspond to respective values for h/K of 0.44, 1.89 and 3.33. To enable flow modeling in the wind tunnel simulation, Kopp and Banks (2013) noted that models at a scale of 1/50 or greater are required to meet the needs for specific racking geometry.
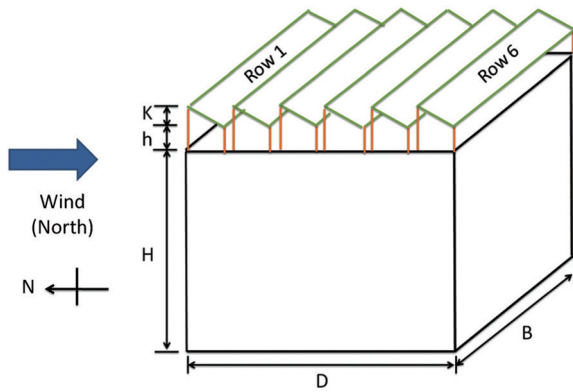
In other words, a large-scale model can accurately reproduce specific geometric features and provide better space resolution in surface pressure pattern. Aly and Bitsuamlak (2013) also indicated a large-scale model can be used to estimate the mean static pressure and 3-s peak loads. For this study, a 1/20 scale model ($B \times D \times H = 50 \times 50 \times 45$ cm) was fabricated. Kopp *et al*. (2012) showed that the building geometry is the dominant factor on wind loads for roof-mounted solar arrays. The effect of mismatch in wind spectrum is expected to be minimized.

Kopp *et al*. (2012) showed that the largest uplift force on roof-mounted solar arrays is observed when the system faces wind direction, especially for row 1. Therefore, the front edge of the present test model faced wind direction and was located 25.3 m from the inlet of the test section. The atmospheric boundary layer (boundary layer thickness, $\delta = 1.65$ m) was accomplished using a combination of spires and floor roughness elements. The mean velocity and turbulence intensity profiles at the center of the test section were measured using a Dantec X-type (55P61) anemometer and the results are shown in Fig. 2. The data agrees with the profiles for

Fig. 1. A schematic drawing of test configuration (by authors).

Table 1. Test configuration (by authors)

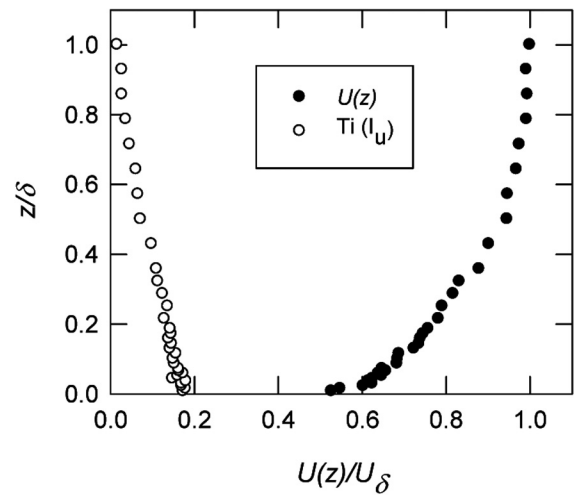| Low-rise building ($B \times D \times H$)	$10 \times 10 \times 9$ m
Solar panel ($L \times W \times t$)	$1.64 \times 0.992 \times 0.04$ m
Solar arrays	6 rows × 10 panels
Tilt angle	25°
Maximum height ($h + K$)	1 m, 2 m, 3 m ($h/K = 0.44, 1.89, 3.33$)

Fig. 2. Velocity and turbulence intensity profiles (by authors).

open terrain with the roughness length of 0.01 m (ESDU, 2001). The freestream velocity, U, and turbulence intensity, T_i, are 12.0 ± 0.1 m/s and 0.3%, respectively. At the roof top (H = 45 cm), the value of T_i is 17%. The Reynolds number, based on the length of the tilted solar panels, Re_L, is 2.52 $\times 10^5$. Fifty-two pressure taps on the upper and the lower surface of each solar array were used for surface pressure measurements. A total of 312 pressure taps were installed on the solar arrays. The SCANVALVE multichannel modules (Model ZOC 33/64Px 64-port) contained net pressure transducers (Model RAD3200). The full-scale range of the sensors is $\pm 2,490$ Pa (or ± 10 inch H_2O) and the accuracy is $\pm 0.15\%$ of the full scale. The sampling rate was 250 Hz and each record contained 32,768 data points.

Irwin *et al*. (1979) demonstrated that the effect of the phase distortion on the measured peak pressures is small for tubes of the order of 60 cm, so the pressure modules were placed inside the model. The pressure taps were connected to flexible polyvinyl chloride tubing that was 60-cm long and which had an internal diameter of 1.1 mm. The mean, p, and fluctuating, σ_p, pressures are non-dimensionalized in terms of the dynamic pressure, q, of the incoming flow, where $C_p = p/q$ and $C_p' = \sigma_p/q$. The normal force coefficient (positive downward), $C_{Fn} = 1/A \int_A \Delta C_p \, dA$, is evaluated by integrating the differential mean surface pressure distributions ($\Delta C_p = C_{p,up} - C_{p,low}$) on the tilted solar panels.

3. Results and Discussion

3.1. Mean and fluctuating pressure contours

The pressure contours for the upper surfaces,

$C_{p,up}$, for R1–R3 are shown in Fig. 3. For a value of $h/K = 0.44$, the lowest value for $C_{p,up}$ is observed near both sides of R1, which indicates that a pair of corner vortices are produced. There is an increase in the value of $C_{p,up}$ for R2 (= -0.85). Further downstream (R3 to R6), the value of $C_{p,up}$ increases gradually and variations in the spanwise direction are minimal. An increase in roof clearance ($h/K = 1.89$ and 3.33) produces stronger suction on R1. The effect of h/K is also evident, which produces an increase in the value of $C_{p,up}$ near the trailing edge of R2. For R3, the counters for $C_{p,up}$ are approximately the same for all three test cases. The pressure contours for the lower surface, $C_{p,low}$, are shown in Fig. 4. Positive values of $C_{p,low}$ are observed on R1. This corresponds to impingement by the incoming flow. There is a suction force on R2 because of the sheltering effect of R1. Further downstream, there is less suction force
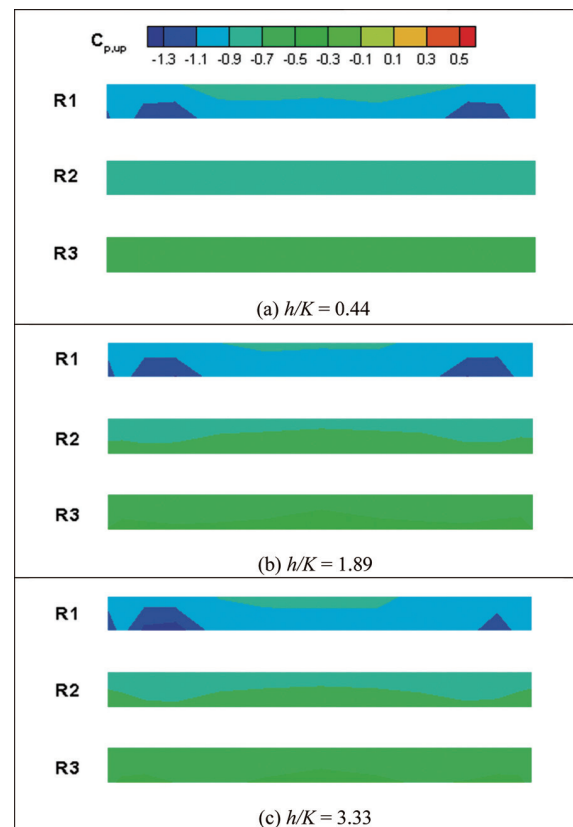

Fig. 3. $C_{p,up}$ contours: (a) $h/K = 0.44$, (b) $h/K = 1.89$ and (c) $h/K = 3.33$ (by authors).
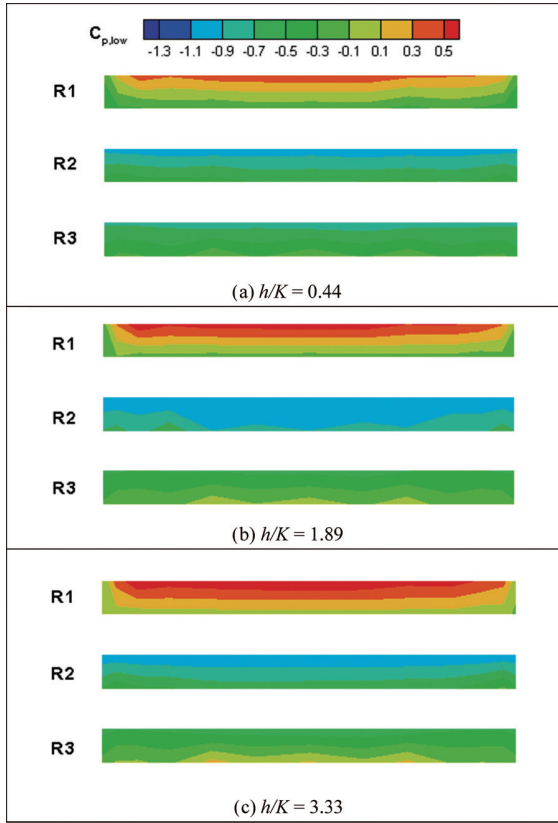
Fig. 4. $C_{p,low}$ contours: (a) $h/K = 0.44$, (b) $h/K = 1.89$ and (c) $h/K = 3.33$ (by authors).

Fig. 5. $C_{p',up}$ contours: (a) $h/K = 0.44$, (b) $h/K = 1.89$ and (c) $h/K = 3.33$ (by authors).

and variation in the value of h/K for $C_{p,low}$ is seen. The amplitude of $C_{p,low}$ near the front edge of R1 and R2 increases when the value of h/K increases. However, there is slight increase in $C_{p,low}$ near the trailing edge of R3.

Fig. 5 shows the fluctuating pressure coefficient on the upper surface, $C_{p',up}$. For a value of $h/K = 0.44$, there are uniform distributions for R1–R3. For values of $h/K = 1.89$ and 3.33, the amplitude of $C_{p',up}$ on R2 and R3 increases significantly, particularly near the front edge. The distribution of the fluctuating pressure coefficient on the lower surface, $C_{p',low}$, is shown in Fig. 6. The value of $C_{p',low}$ is higher for R2 (the maximum value of $C_{p',low} = 0.62$ for $h/K = 3.33$) and the amplitude increases when the value of h/K increases. Wind-induced vibrations require caution.
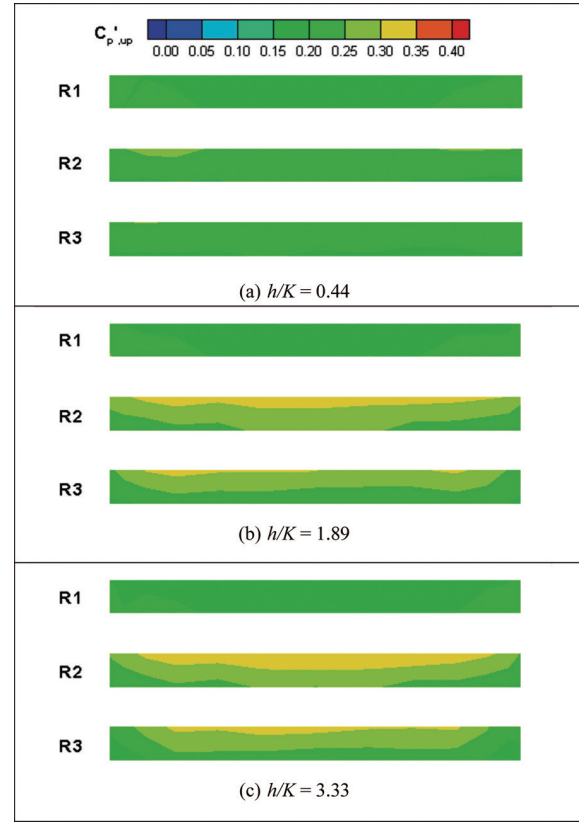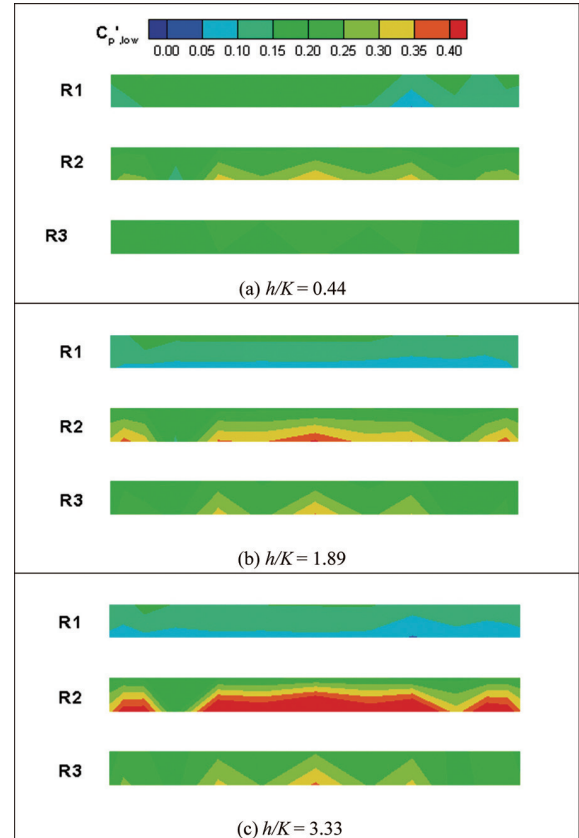

Fig. 6. $C_{p',low}$ contours: (a) $h/K = 0.44$, (b) $h/K = 1.89$ and (c) $h/K = 3.33$ (by authors).

3.2. Longitudinal pressure distributions

The $C_{p,up}$ distribution on the central line ($y/B = 0.5$) of R1–R6 is shown in Fig. 7a. The origin of the coordinates ($x/D = 0$ and $y/B = 0$) is located at the corner of the flat roof. The lowest value for $C_{p,up}$ on R1 corresponds to flow separation on the upper surface of the tilted panels. The value of $C_{p,up}$ increases from R2 to R5 and there is a small difference between the values for R5 and R6. Variations of $C_{p,up}$ show similar trends with previous studies (Pratt & Kopp, 2013; Kopp *et al.*, 2012) at a lower value of h/K (= 0.18-0.28). The effect of h/K is also evident. When the value of h/K increases, there is stronger suction on R1 and the value of $C_{p,up}$ on R2–R4 increases downstream. However, the opposite trend is true for R6. The $C_{p,low}$ distributions on the lower surface are shown in Fig. 7b. It is seen there is a positive value for
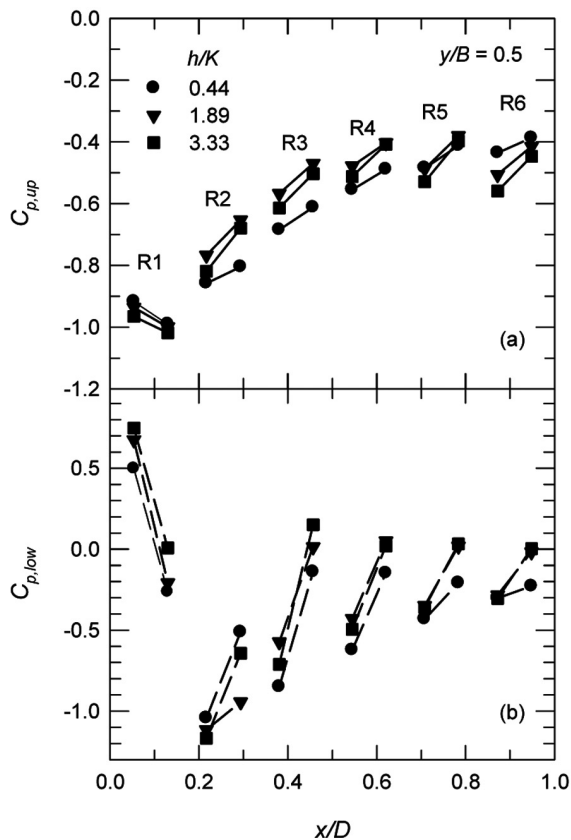
$C_{p,low}$ near the front edge of R1 which corresponds to impingement of the incoming flow. The suction force near the front edge of R2–R6 is greater than that near the trailing edge. In other words, the tilted panels are subject to greater wind load near the front edge. For values of $h/K = 1.89$ and 3.33, there is an increase in the value of $C_{p,low}$. Further, the peak pressures are estimated using the Cook-Mayne method (1980) and the results are shown in Fig. 8. Variations in $C_{p,up(peak)}$ and $C_{p,low(peak)}$ show similar trends as those for $C_{p,up}$ and $C_{p,low}$. However, the values of $C_{p,up(peak)}$ are lower than those of $C_{p,up}$. The lowest $C_{p,low(peak)}$ is observed at $x/D = 0.217$ of R2. The effect of h/K is more evident on $C_{p,low(peak)}$ than on $C_{p,low}$. To determine the net uplift force, the ΔC_p distributions at $y/B = 0.5$ are shown in Fig. 9. For a value of $h/K = 0.44$, the most negative value for ΔC_p on R1 represents the greatest uplift force, in comparison with those for R2–R6. It is
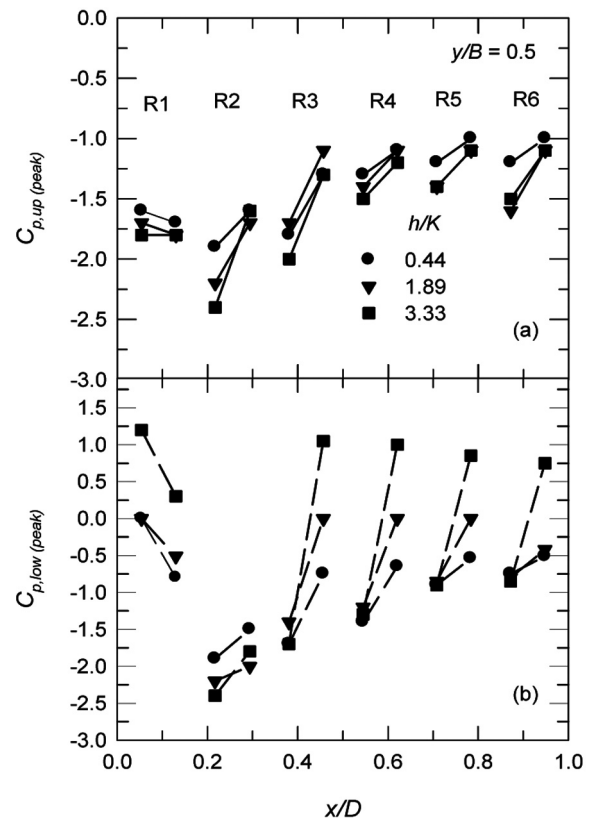
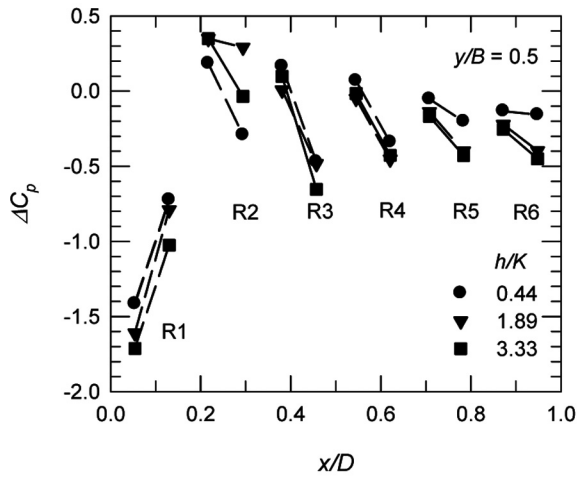Fig. 7. Mean pressure distributions for $y/B = 0.5$ (by authors).

Fig. 8. Peak pressure distributions for $y/B = 0.5$ (by authors).

C. C. Chou, C. Y. Chung, K. M. Chung: The Effect of Roof Clearance on Wind Loads
for Solar Arrays on a Low-rise Building

51

Fig. 9. ΔC_p distributions for $y/B = 0.5$ (by authors).

also noted that the wind load is minimized on R5 and R6. It is also seen that the value of h/K has an effect. The uplift force increases when there is an increase in the value of h/K, but not for R2.

The distributions of $C_p{}'$ at $y/B = 0.5$ are shown in Fig. 10. On the upper surface ($C_{p',up} = 0.17$–0.29
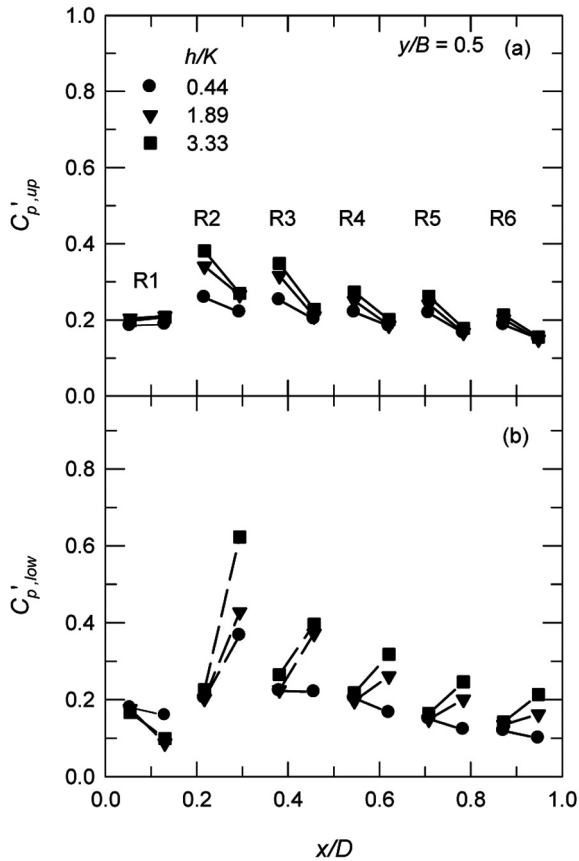

Fig. 10. Fluctuating pressure distributions for $y/B = 0.5$ (by authors).

for $h/K = 0.44$), fluctuations in the loads are more significant near the front edge of each panel and the amplitude of the fluctuation decreases slightly downstream at R6. An increase in the value of h/K results in larger pressure fluctuations and the largest value of $C_{p',up}$ is observed at R2 for a value of $h/K = 3.33$. On the lower surface, the value of $C_{p',low}$ near the front edge of R1 and R3–R6 is higher than the value near the trailing edge for a value of $h/K = 0.44$, as shown in Fig. 10b. However, the opposite trend is true for values of $h/K = 1.89$ and 3.33. The peak value for $C_{p',low}$ ($= 0.62$) is observed on R2. This may be due to upward movement of wind between the flat roof and the solar array. Future study using numerical simulation is required to detail the flowfield.

3.3. Spanwise pressure distributions

The spanwise pressure distributions, C_{sp}, near the front edge of R1, R2 and R6 (0.24L) are shown in Fig. 11. On the upper surface, the amplitude of $C_{sp,up}$ increases significantly from R1 to R6, which indicates a significant reduction in the uplift force. The value of h/K has an effect, particularly near the side edges of R6 ($y/B \approx 0.1$ and 0.9). An increase in the value of h/K results in greater suction force on the upper surface. On the lower surface, impingement of the incoming flow results in a compressive force on R1, but not near the side edges. The uplift force increases when the value of h/K increases. There is a sheltering effect on R2 and R6. The difference in pressure between the upper and lower surfaces is significantly lower than the difference for R1. These results are in agreement with those of Radu et al. (1986, 1989). It is worthy of note that the effect of h/K on the lower surface of R6 is minimal.

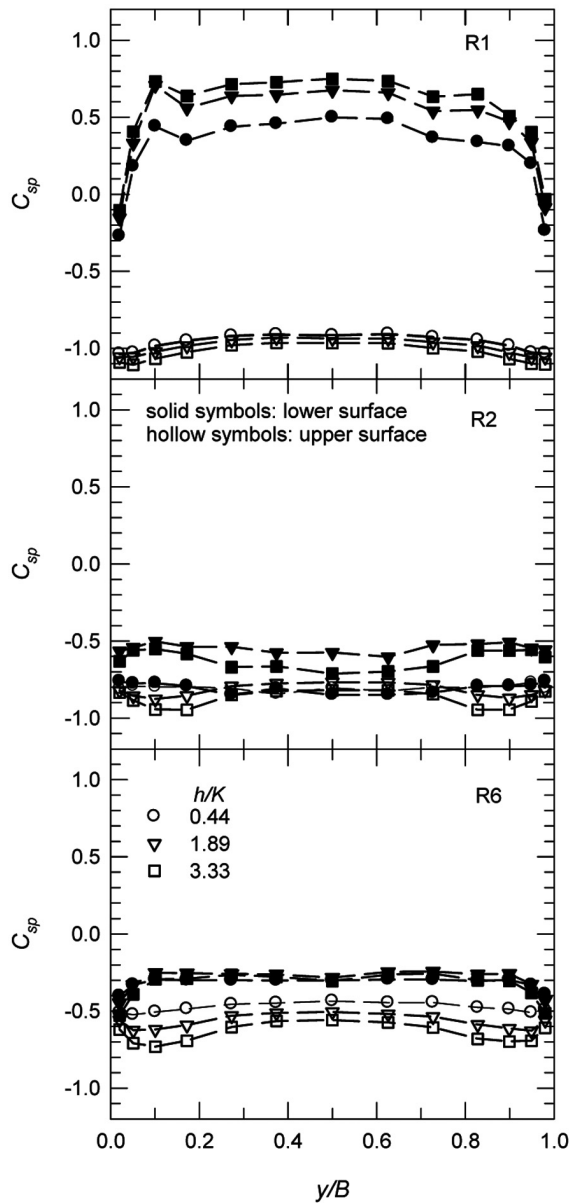Fig. 12 shows the C_{sp} distribution at 0.76L, near the trailing edge of solar arrays. The value of

Fig. 11. C_{sp} distributions at 0.24L (by authors).

Fig. 12. C_{sp} distributions at 0.76L (by authors).

$C_{sp,up}$ on R1 near the centerline ($\approx$ -0.99) is slightly less than that at 0.24L ($\approx$ -0.90), where there is also an increase in the value of h/K. On R2, there are significant variations and the amplitude of $C_{sp,up}$ for values of $h/K = 1.89$ and 3.33 is greater than that for a value of $h/K = 0.44$, which indicates a reduction in the suction force. The h/K effect is minimal for R6 and the amplitude of $C_{sp,up}$ is greater than that at 0.24L. On the lower surface, there is an interaction between the incoming flow and the roof clearance. The suction force on R1 is less than that at 0.24L, particularly for a value of $h/K = 3.33$. On R2, the
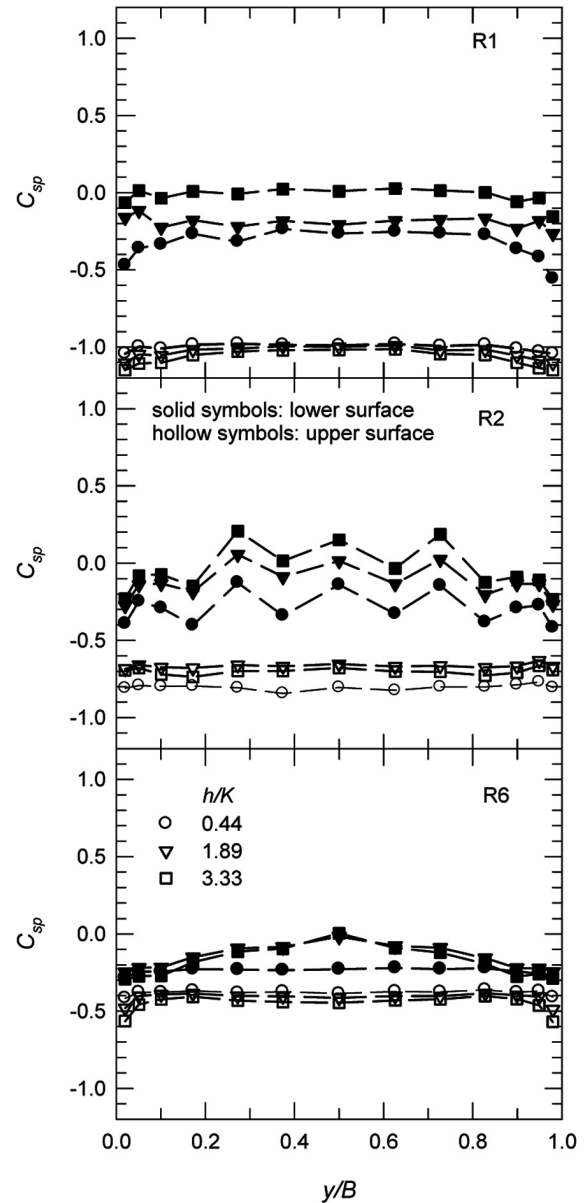
spanwise pressure distributions have a serrated form. The sheltering effect of R1 may have a major role. Further downstream, such as at R6, there is less significant variation in the spanwise pressure distribution.

The spanwsie distributions of the pressure fluctuations on the upper surface at 0.24L are shown in Fig. 13. For a value of $h/K = 0.44$ and R1, the value of $C_{sp',up}$ near the side edges is greater than that in the central region. The distributions on R2 and R6 are fairly flat. The value of h/K has a more significant effect on R2. On the lower surface
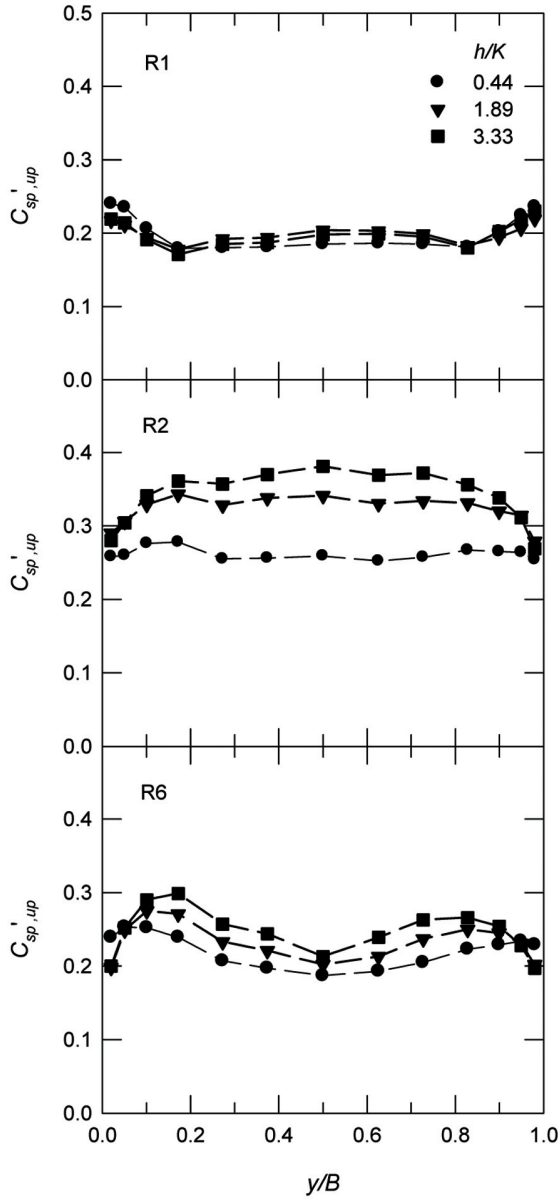
Fig. 13. $C_{sp',up}$ distributions at 0.24L (by authors).

Fig. 14. $C_{sp',low}$ distributions at 0.76L (by authors).

at 0.76L, variations in the pressure fluctuations in the spanwise direction for R1 are minimal. The value $C_{sp',low}$ is reduced when there is an increase in roof clearance, as seen in Fig. 14. The serrated form of $C_{sp',low}$ distributions is similar to those for $C_{sp,low}$. The peak value of 0.62 is observed for a value of $h/K = 3.33$ at $y/B = 0.5$. Wind-induced vibrations require caution. The value of $C_{sp',low}$ for R6 is relatively low, except at $y/B = 0.5$.

3.4. The normal force on solar arrays
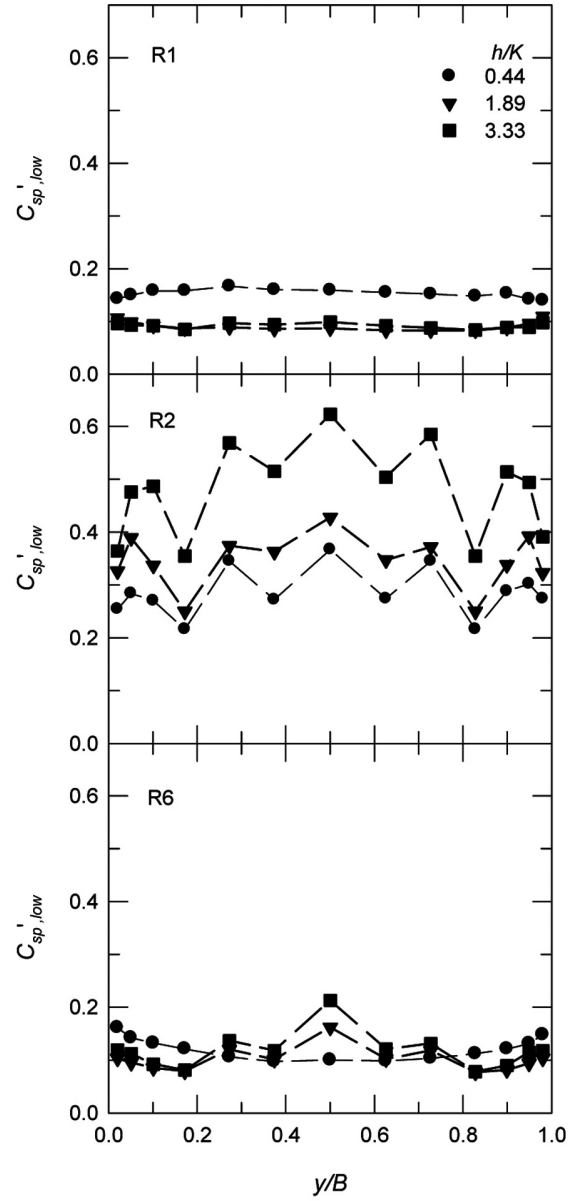
The normal force on the tilted panels, C_{Fn}, is calculated by integrating the mean upper and lower surface pressures. Since there is a limited number of pressure taps on the upper and lower surfaces, the results are only qualitative. A more negative value for C_{Fn} represents a greater uplift force. For tilt angle of 5°, Kopp (2014) showed that there is a substantial increase in the normal force when $h = 1.02$ m, in comparison with that $h = 0.15$ m. For a value of $h/K = 0.44$ or $h = 1$ m, as shown in Fig. 15, R1 is subject to the greatest uplift force ($C_{Fn} = -0.93$). There is a small variation from R2 to R6, where the value of C_{Fn} ranges from -0.08 to -0.14.
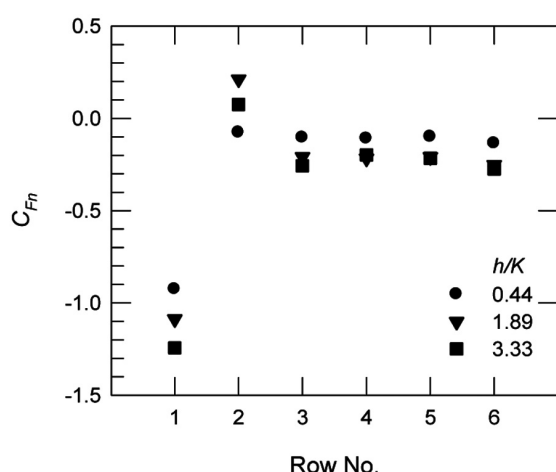
Fig. 15. Normal force coefficient for solar arrays (by authors).

When the value of h/K increases, the value of C_{Fn} on R1 (= -1.09 and -1.24 for h/K = 1.89 and 3.33 or h = 2 and 3 m, respectively) decreases when there is a greater roof clearance and positive values are observed on R2 (downward force). The effect of the value of h/K on R3–R6 is minimal, but there is greater uplift force than when the value of h/K = 0.44.

4. Conclusions

This study determines the effect of roof clearance on wind loads for a PV system on a low-rise building. When facing into the direction of the wind, the uplift force is greatest on the first solar array. There is a 30% increase when the roof clearance is increased. Wind loads on the downstream solar arrays are much less than that on the first solar array, because the first row provide a degree of sheltering. The amplitude of the pressure fluctuations on the second to sixth arrays increases when the roof clearance is increased. Peak fluctuating pressure coefficient reaches a value of 0.62 on the lower surface of the second solar array. This corresponds to vortex shedding by the first solar array. Wind-induced vibrations require caution.

Acknowledgments

References

Aly, A. and G. Bitsuamlak, 2013. Aerodynamics of ground-mounted solar panels: Test model scale effects. Journal of Wind Engineering and Industrial Aerodynamics, 123, 250-260.

ASCE 7-10, 2010. Minimum Design Loads for Buildings and Other Structures. American Society of civil Engineers, Reston, Virginia.

BOEMOEA, 2016. Solar PV Two-Year Promotion Project. Bureau of Energy, Ministry of Economic Affairs (BOEMOEA), Taipei, Taiwan, Republic of China. http://www. moeaboe.gov.tw/ECW/english/ content/ Content. aspx?menu_id=5492 (accessed on December 25, 2018).

BOEMOEA, 2017. 2016 Energy statistical data book. Bureau of Energy, Ministry of Economic Affairs (BEMOEA). Taipei, Taiwan, Republic of China.

Cao, J., A. Yoshida, P. K. Saha and Y. Tamura, 2013. Wind loading characteristics of solar arrays mounted on flat roofs. Journal of Wind Engineering and Industrial Aerodynamics, 123, 214-225.

Chen, J. M. and Y. Fang, 1996. Strouhal numbers of inclined flat plates. Journal of Wind Engineering and Industrial Aerodynamics, 61, 99-112.

Chou, C. C., K. M. Chung and K. C. Chang, 2014. Wind loads of solar water heaters: Wind

incidence effect. Journal of Aerodynamics, 2014, Article ID 835091, 10 pages.

Chung, K. M., K. C. Chang and C. C. Chou, 2011. Wind loads on residential and large-scale solar collector models. Journal of Wind Engineering and Industrial Aerodynamics, 90, 59-64.

Chung, K. M., C. C. Chou, K. C. Chang and Y. J. Chen, 2013. Effect of a vertical guide plate on the wind loading of an inclined flat plate. Wind and Structures, 17(5), 37-552.

Cook, N. J. and J. R. Mayne, 1980. A refined working approach to the assessment of wind loads for equivalent static design. Journal of Wind Engineering and Industrial Aerodynamics, 6, 125-137.

ESDU, 2001. Characteristics of atmospheric turbulence near the ground. Part II single point data for strong winds (neutral atmosphere). Engineering Sciences Data Unit, Item 85020 Issued October 1985, with Amendments A to G.

Irwin, H. P. A. H. and K. R. Cooper, R. Girard, 1979. Correction of distortion effects caused by tubing systems in measurements of fluctuating pressures. Journal of Wind Engineering and Industrial Aerodynamics, 5(1-2), 93-107.

Kaohsiung City, 2017. Build code for PV systems. https://outlaw.kcg.gov.tw/LawQuery.aspx (accessed on July 29, 2019)

Kopp, G. A., D. Surry and K. Chen, 2002. Wind loads on a solar array. Wind and Structures, 5(5), 393-406.

Kopp, G. A., S. Farquhar and M. Morrison, 2012. Aerodynamic mechanisms for wind loads on tilted, roof-mounted, solar array. Journal of Wind Engineering and Industrial Aerodynamics, 111, 40-52.

Kopp, G. A. and D. Banks, 2013. Use of the wind tunnel test method for obtaining design wind loads on roof-mounted solar array. Journal of Structural Engineering, 139(2), 284-287.

Kopp, G. A., 2014. Wind loads on low-profile, tilted, solar arrays placed on large, flat, low-rise building roofs. Journal of Structural Engineering, 140(2), Article 04013057.

Matty, R. R., 1979. Vortex shedding from square plates near a ground plane: an experimental study. Master thesis, Texas Tech University.

Mauthner, F. W. and M. Spörk-Dür, 2019. Solar heat worldwide. AEE-Institute for Sustainable Technologies, Gleisdorf, Austria.

Naeiji, A., F. Raji and I. Zisis, 2017. Wind loads on residential scale rooftop photovoltaic panels. Journal of Wind Engineering and Industrial Aerodynamics, 168, 228-246.

Pratt, R. N. and G. A. Kopp, 2013. Velocity measurements around low-profile, tilted, solar arrays mounted on large flat-roofs, for wall normal wind direction. Journal of Wind Engineering and Industrial Aerodynamics, 123, 226-238.

Radu, A. and E. Axinte, 1986. Theohari, C. Steady wind pressures on solar collectors on flat-roofed building. Journal of Wind Engineering and Industrial Aerodynamics, 23, 249-258.

Radu, A. and E. Axinte, Wind forces on structures supporting solar collectors. Journal of Wind Engineering and Industrial Aerodynamics, 32, 93-100.

Stathopoulos, T., I. Zisis and E. Xypnitou, 2014. Local and overall wind pressure and force coefficients for solar panels. Journal of Wind Engineering and Industrial Aerodynamics, 125, 195-206.

Strobel, K. and D. Banks, 2014. Effects of vortex shedding in arrays of long inclined

flat plates and ramifications for ground-mounted photovoltaic arrays. Journal of Wind Engineering and Industrial Aerodynamics, 133, 146-149.

Voigt, C., 2016. The compliance and implementation mechanism of the Paris Agreement. Review of European Comparative & International Environmental Law, 25(2), 161-173.

Warsido, W. P., G. T. Bitsuamlak, J. Barata and A. G. Chowdhury, 2014. Influence of spacing parameters on the wind loading of solar array. Journal of Fluids and Structures, 48, 295-315.

安裝高度對光電系統風負載之效應

周晉成[1]　鍾政洋[1]　鍾光民[2*]

摘　要

再生能源應用為臺灣主要的能源政策之一，針對光電系統的推廣，部分縣市放寬安裝高度的限制(最高可離屋頂樓板6米)，但是臺灣地處颱風帶，系統設計必須考量風負載。本實驗研究探討在一低層建築屋頂光電系統的風負載特性(傾斜角25度、6排陣列)，於一邊界層風洞進行1:20模型測試，量測模型表面平均及擾動壓力分佈，正向力則計算上下板面壓差之積分。結果顯示，當風向角為零度時，面對來流之第一排陣列承受最大正向力，遮蔽效應則降低第二至六排陣列之正向力，擾動壓力極值出現在第二排陣列。當安裝高度升高，第一排陣列之正向力(提高30%)及第二至六排陣列之擾動壓力(最大壓力擾動係數達0.62)皆隨之增加，光電板因氣流導致振動的現象，必須在系統設計時一併考量。

關鍵詞：安裝高度，風負載，太陽能陣列，低層建築，再生能源